International Journal of Nanoelectronics and Materials
Volume 11 (Special Issue) Nov 2018 2018 [59-70]

Effect of Surfactant Concentrations on Pore Characteristics of Mesoporous Carbonated Hydroxyapatite Prepared by Soft-Templating Hydrothermal Method

N. F. Mohammad[1, 2,*], R. Othman[3], A. A. Abdullah[1] and F. Y. Yeoh[2]

[1] *Programme of Biomedical Electronic Engineering, School of Mechatronic, Universiti Malaysia Perlis, Pauh Putra Campus, 02600 Arau, Perlis, Malaysia.*
[2] *School of Materials and Mineral Resources Engineering, Engineering Campus, Universiti Sains Malaysia, 14300 Nibong Tebal, Penang, Malaysia.*
[3] *Faculty of Manufacturing Engineering, Universiti Teknikal Malaysia, Melaka, Hang Tuah Jaya, 76100 Durian Tunggal, Melaka.*

ABSTRACT

Mesoporous carbonated hydroxyapatite is a promised material for the application in drug delivery. Mesoporous carbonated hydroxyapatite (CHA) was synthesised through a hydrothermal co-precipitation method using different concentration (1.7, 7, 10 and 14 mM) of non-ionic surfactant P123 as a pores template. The crystalline phase, chemical composition, morphology and pore size distribution of mesoporous CHA were analysed using various materials characterisation techniques. The presence of mesopores as an array of pore channels in the synthesised sample were confirmed using transmission electron microscope. The optimum pore characteristics (i.e. surface area = 78 m^2g^{-1}, pore size = 27 nm and pore volume = 0.542 nm) of mesoporous CHA was obtained when surfactant concentration (1.7 mM) was maintained closed to critical micelle concentration (CMC), 0.0044 mM.

Keywords: Mesoporous, Nanoporous, Carbonated Hydroxyapatite, Surfactant, Drug Delivery.

1. INTRODUCTION

The main inorganic component of human bones and teeth mineral is biological apatite. Biological apatite are the impure and non-stoichiometric version of hydroxyapatite (HA) [1, 2] have low crystallinity and contains several ions (such as CO_3^{2-}, Mg^{2+}, Na^+, Fe^{2+}, HPO_4^{2-}, F^- and Cl^-) substituted in the HA lattice, where carbonate (CO_3^{2-}) is the most abundant species. Therefore, biological apatite also referred as carbonated hydroxypatite (CHA). The content of carbonate in human bone mineral is about 2-8 wt% depending on the individual age [3-6].

Past researches have shown that, mesoporous CHA exhibits a great performance as a drug carrier [7-14]. The International Union of Physical and Applied Chemistry (IUPAC) classified pores as micropores (pore size < 2 nm), mesopore (2 nm < pore size < 50 nm) mesopores and macropores (pore size > 50 nm [15, 16]. With the development of nanotechnology, micro-, meso-, and macropores materials can also be described as nanoporous materials, because their pore sizes are less than 100 nm, which fall within the nanoscale range [17]. ISO classification (ISO/TS 80004-1:2010) states that nanoporous materials are materials possessing pores of diameters between 1 nm and 100 nm [18].

*Corresponding Author: *farahiyah@unimap.edu.my*

However, so far, study on mesoporous CHA for drug delivery application is very limited and most of the mesoporous CHA has been fabricated by hydrothermal [11, 13] and emulsion [8, 14] method using calcium carbonate microsphere as a hard sacrificial template. Hydrothermal hard-templating method has been used to synthesise mesoporous CHA for drug delivery systems. Guo *et al*. [9-12] had implemented this method by using $CaCO_3$ microspheres serve as the sacrificial template to synthesise mesoporous carbonated hydroxyapatite microspheres (MCHMs). The MCHMs with a particle size of about 5 μm has been fabricated hydrothermally by soaking $CaCO_3$ microspheres in a disodium hydrogen phosphate solution at 140°C in Teflon line steel autoclave. The pore sizes of MCHMs mainly distributed at 4.5-14.0 nm. The specific surface area and pore volume of MCHMs are 29.3-35.1 m^2g^{-1} and 0.049-0.083 cm^3g^{-1}. The MCHMs microspheres synthesised has been used to load various type of drug such as vancomycin [11] and gentamicin [13]. MCHMs demonstrated higher drug loading efficiency of 70-75% with gentamicin. The gentamicin-loaded MCHMs display a slow and sustained release of gentamicin up to 6 days compared to conventional hydroxyapatite particles [13]. However, gentamicin-loaded MCHMs exhibit a burst-release effect at the first 6 hours in which over 90% of the loaded drugs released during this period.

Chemical precipitation and the hydrothermal method also has been used as a main process in soft-templating technique in which macromolecules act as a soft temporary template or nucleation centres to modulate the morphology, introduce pores and increase crystallinity. The soft-template method able to produce pores in mesopore size and control pore size. Moreover, it involves simple synthesis procedure, easily obtained chemicals and simple apparatus needed for the experiment. Therefore, the soft-template method is a promising method to be use in the synthesis of mesoporous carbonated hydroxyapatite (HA). The surfactant based template system is the most common soft-templating technique used to introduce pores within the nanoparticles.

Surfactants can be classified into four types, as non-ionic, cationic, anionic, and amphoteric based on the composition of their hydrophylic head. Amphiphilic molecules of the surfactants form micelles with a designated shape through self-assembly as soon as their concentration exceeds the critical micelle concentration (CMC) [19]. In the solution mixture of Ca^{2+} and PO_4^{3-}, micelles act as a template for crystal growth at a certain concentration and pH [20, 21].

Previously, ionic type surfactants were commonly used in the synthesis of hydroxyapatite (HA) [20, 22]. Unfortunately, ionic surfactants such as cationic alkyltrimethylammonium, anionic alkylsulfonates or alkylphosphates have two main disadvantages as pore templates: a) the wall thickness of the pores produced is between 0.8-1.3 nm, which is a limitation regarding stability for catalysis, (b) limited pore size can be created by the surfactant [23, 24]. In order to overcome these limitations, non-ionic surfactants such as poly (alkaline oxide) triblock co-polymers, e.g. P123 and F127, has been used as structure directing agents. Poly (alkaline oxide) triblock co-polymers, such as poly (ethylene oxide) - poly (propylene oxide) - poly (ethylene oxide) (PEO-PPO-PEO), are excellent candidates for structure directing agents because of their mesostructural ordering properties, amphiphilic character, commercial availability and biodegradability [25].

2. METHODOLOGY

2.1 Materials

The chemicals used as the calcium and phosphate precursor were calcium nitrate tetrahydrate ($Ca(NO_3)_2.4H_2O$) and diammonium hydrogen phosphate ($(NH_4)_2.HPO_4$) respectively. Ammonium hydrogen carbonate (NH_4HCO_3) was used as a carbonate precursor. Non-ionic triblock co-polymer Pluronics® P123, ($PEO_{19}PPO_{69}$ PEO_{19}) donated by BASF, USA were used as the structure directing agent for the pore template. Besides that, pH of the mixture was maintained at pH 11 throughout the mixing process using sodium hydroxide (NaOH).

2.2 Sample Preparation

Mesoporous carbonated hydroxyapatite samples with designed surfactant concentrations of 1.7, 7, 10 and 14 mM was prepared by dissolving 1 g, 4 g, 6 g and 8 g of P123, respectively in 100 mL of deionised water (DI water), followed by the addition of 9.45 g of $Ca(NO_3)_2.4H_2O$. The surfactant-calcium mixed solution was then stirred for 30 minutes to obtain a clear micellar solution. In the meantime, 3.17 g of $(NH_4)_2.HPO_4$ was dissolved in 60 mL of DI water. Then, 3.795 g of ammonium hydrogen carbonate (NH_4HCO_3) was added to the solution as a carbonate source. The final solution was prepared by dripping phosphate-carbonate mixture slowly into surfactant-calcium solution and continuously stirs the mixtures. Throughout the mixing process, pH of solution was constantly maintained at pH 11. The white solutions then transferred into a Teflon® bottle and aged at 120°C for 24 hours. White precipitates were obtained by centrifuged the white solution at 3000 rpm for 20 minutes. Next, the precipitate washed and centrifuged repeatedly for five times with deionized water and dried in an oven at 100°C for 24 hours. The dried precipitate was grinded into fine powders and further calcined at 550 °C for 6 hours in a furnace. The obtained products were labelled as CHA-1P, CHA-4P, CHA-6P and CHA-8P. Nonporous carbonated hydroxyapatite (CHA-0P) was prepared using the same conditions but without P123 acted as a control sample.

2.3 Sample Characterization

The phase composition of the samples were analysed by using X-ray Diffraction (XRD, Bruker AXS D8) diffractometer using Cu Kα radiation (λ = 0.15406 nm) over the range of 10° ≤ 2θ ≤ 90. According to Landi *et al*. [26], the crystallinity degree corresponding to the fraction of crystalline phase present in the examined volume was calculated using Equation 1;

$$X_c = 1 - \frac{V_{112/300}}{I_{300}} \quad (1)$$

where X_c is the fraction of crystalline phase; I_{300} is the intensity of (300) reflection; $V_{112/300}$ is the intensity of hollow between (112) and (300) diffractions , which completely disappears in non-crystalline samples.

The formation of carbonated hydroxyapatite was confirmed using Fourier Transform Infrared (FTIR) spectra (Perkin Elmer Spectrum One spectrophotometer) in the range of wave numbers of 4000-400 cm^{-1}. Prior to FTIR characterization, the samples were mixed with potassium bromide (KBr), ground into fine powder and compacted into a transparent disc for measurement. The Zeiss SUPRA 35VP field emission scanning electron microscopy (FESEM) was used to observed the morphological and nanostructure of the samples. The mesoporous structures of the samples were verified using high-resolution transmission electron microscope (HRTEM, Technai™, G2 F20 S-Twin). Nitrogen adsorption-desorption isotherms were measured with a Quanta chrome Autosorb® IQ. The specific surface area of the samples was measured based on Brunauer-Emmett-Teller (BET) equation. The pore size distribution (PSD) of the samples was derived from the desorption branches of the isotherms using Barrett-Joyner-Halenda (BJH) model.

3. RESULTS AND DISCUSSION

3.1 Phase and Crystallinity of the Materials

Figure **1** shows the X-ray diffraction patterns of the samples synthesised at various concentration of P123. In all samples, the characteristic peaks appearing in the XRD pattern are attributed to CHA reflections and no characteristic peaks of impurities are observed which are well consistent with

PDF Number 98-010-1164. The XRD patterns show that the crystal structure of CHA is the hexagonal $P6_3/m$. The three main characteristic peaks of CHA at 2θ = 25.6, 31.8 and 33° [27-31] which can be indexed at (002), (211) and (300), were clearly observed in all XRD patterns.

There are no significant differences observed in the XRD pattern between the samples synthesise using various concentrations (CHA-1P, CHA-4P, CHA-6P and CHA-8P). The result shows that variations of surfactant concentration did not affect the purity of the CHA. On the other hand, the sample without surfactant, CHA-0P has narrower and sharper XRD pattern compared to other samples. The intensity of the diffraction peaks of sample synthesise using P123 is much lower than without P123. In a CHA-0P pattern, the intensity of diffracted X-rays corresponding to (002) planes are 1402 units. Meanwhile, in the case of CHA-1P, the intensity of diffracted X-rays corresponding to (002) planes are 577 units. The crystallinity of the CHA samples synthesised at various P123 concentrations is further investigated by the crystallinity values from XRD results. The crystallinity of the materials that shown in Table 1 were calculated using Equation 1.

The sample with no surfactant, CHA-0P has the highest crystallinity compared to other samples. However, with the addition of surfactant, the crystallinity reduces. The presence of P123 during formation of CHA crystal was thought to disturb the long-range order of the crystal structure and thus, giving a lower crystallinity fraction. This finding is in agreement with the XRD pattern in Figure 1 where in P123, XRD peaks are broader than without P123.

As shown in Table 1, crystallinity of the mesoporous CHA increases as the concentration of P123 increases. This most probably due to P123 which acts as a regulating agent in crystallization and growth of CHA particles during the synthesis process [32]. Self-assembly of the micelles takes place as the P123 concentration is larger than critical micelle concentration (CMC) which is 0.0044 mM [33]. Therefore, P123 more likely to form micelles as the concentration increases compared to the lower concentration. This result an increase in the number of template for CHA precipitation hence more CHA crystal formed**.**

3.2 FTIR Analysis

The FTIR spectra of all samples were consistent (
Figure **2**) whereby the characteristic bands for CHA were present in the samples. The band at 3568 cm^{-1} is belonged to OH^{-1} group from the H_2O [31, 34]. The bands at 1050, 962 and 470 cm^{-1} ascribed to the stretching vibration (v_3) of the phosphate (PO_4^{3-}) ions, and the absorption bands at 603 and 567 cm^{-1} are attributed to the bending vibration (v_4) of the phosphate (PO_4^{3-}) ions which similar with others researches work [31, 34]. The absorption band at approximately 1092 cm^{-1} due to HPO_4^{2-} group indicates that carbonated hydroxyapatite (CHA) is calcium deficient apatite [12]. The characteristic bands of CO_3^{2-} for B-type CHA were recognized at 1467, 1416, and 872 cm^{-1} as shown in
Figure **2** [31, 34].

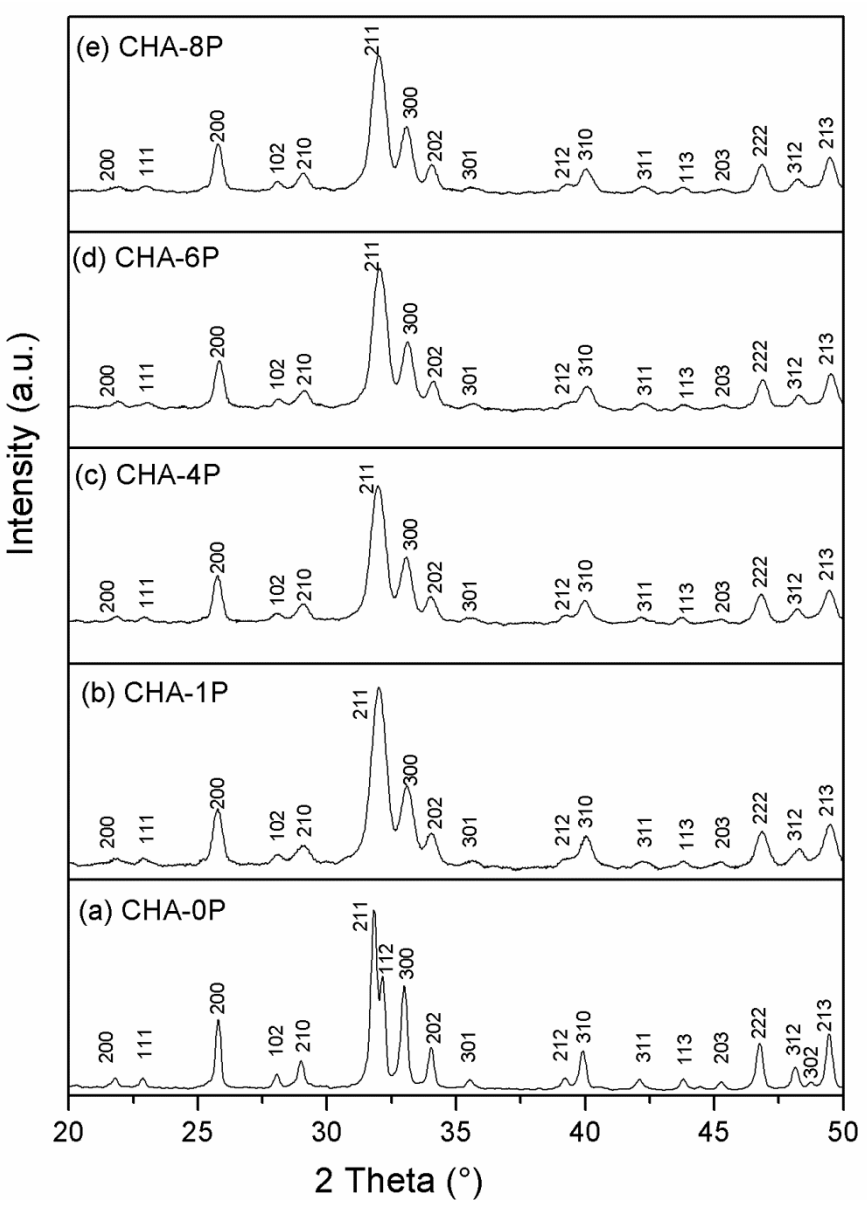

Figure 1. XRD patterns of CHA samples synthesised with and without surfactant, (a) No surfactant (CHA-0P), (b) 1.7 mM P123 (CHA-1P), (b) 7 mM P123 (CHA-4P), (c) 10 mM P123 (CHA-6P) and (d) 14 mM P123 (CHA-8P).

Table 1 Crystallinity of mesoporous CHA synthesises using different concentration of surfactant

Sample	Concentration of P123 (mM)	Crystallinity, Xc (%)
CHA-0P (control)	0	84
CHA-1P	1.7	52
CHA-4P	7	58
CHA-6P	10	59
CHA-8P	14	60

Overall, it was confirmed that B-type carbonated hydroxyapatite was produced and no other ionic compound was formed regardless of different concentration of surfactant was used. After calcination, no sign of surfactant presence was detected in the spectra validating a complete surfactant removal of all the samples leaving a pure CHA samples.

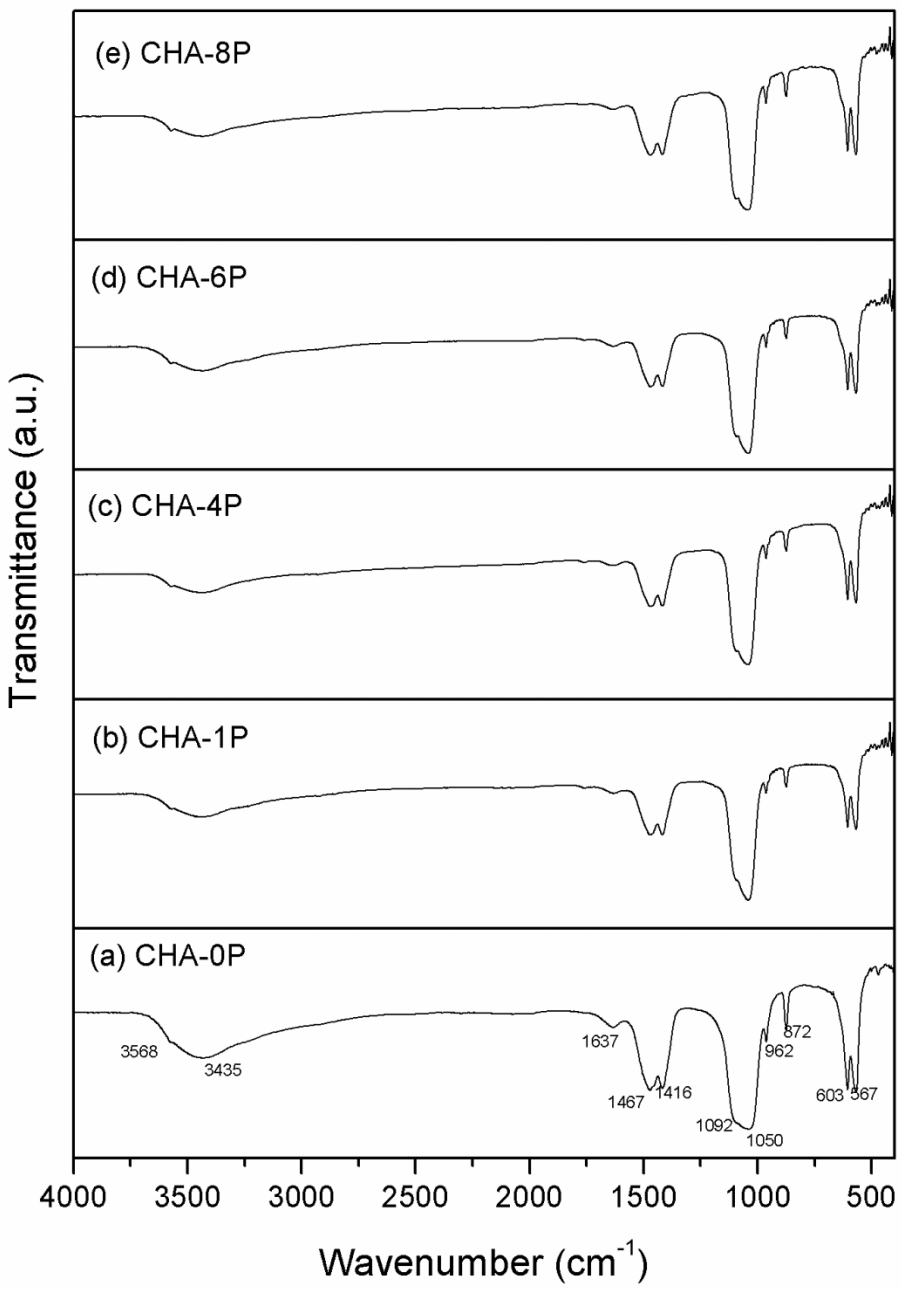

Figure 2. FTIR spectra of CHA-0P, CHA-1P, CHA-4P, CHA-6P and CHA-8P samples.

3.3 Morphology and Pore Characterisation of Mesoporous CHA

SEM images of sample CHA-0P, CHA-1P, CHA-4P, CHA-6P and CHA-8P are shown in

Figure **3**. It can be observed from each individual image that all samples consist of agglomerated spherical like nanoparticles. However, TEM (

Figure **4**) revealed that the nanoparticles are in irregular shape. This most probably because the nanoparticles were highly agglomerated, therefore, spherical-shaped mesoporous CHA particles observed under SEM were not clearly observed by the TEM. The formation of fine agglomerates most probably due to Van der Waals force attraction between the nanoparticles.

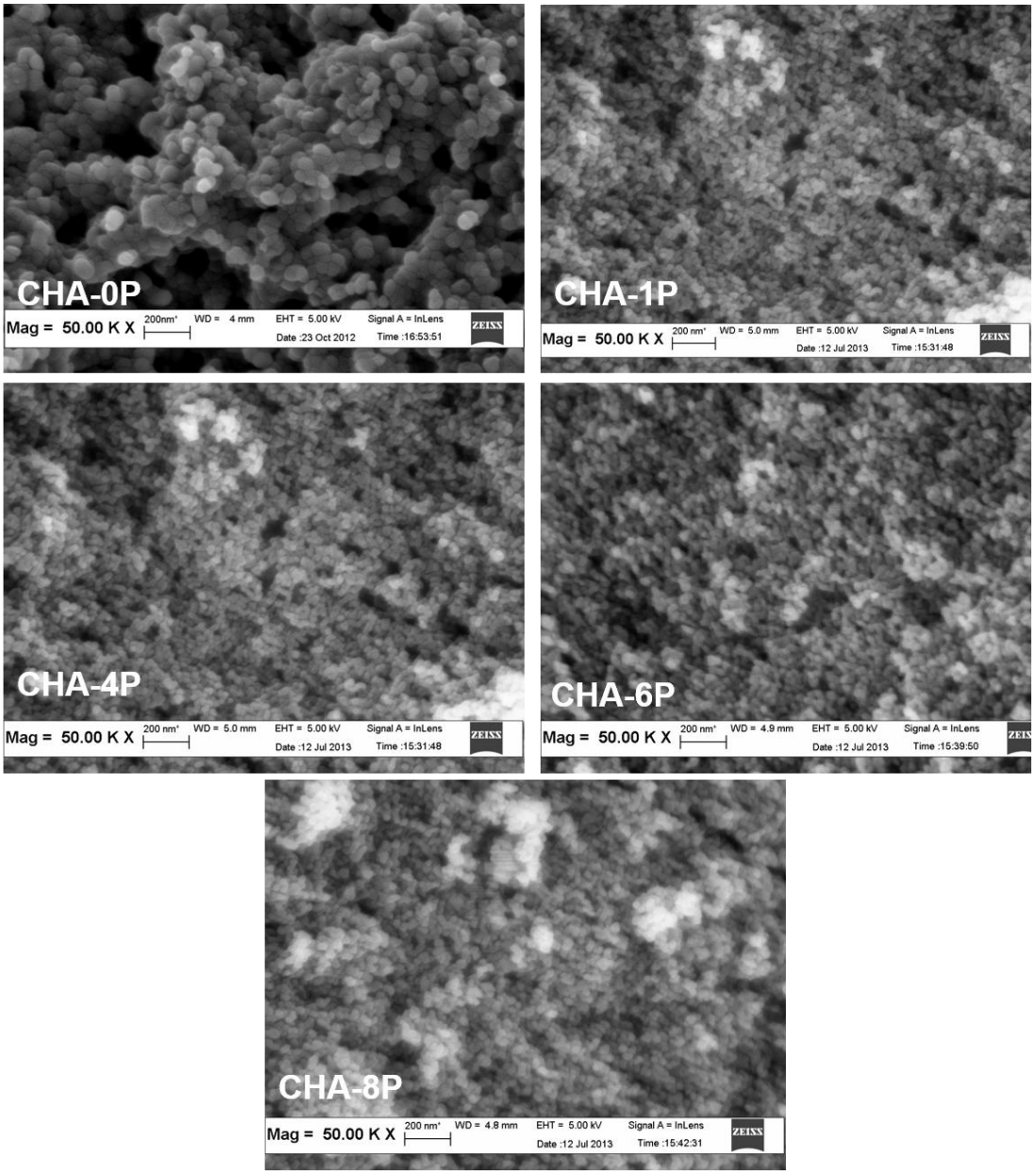

Figure 3. SEM images of CHA-0P, CHA-1P, CHA-4P, CHA-6P and CHA-8P.

As shown in

Figure **4**, mesopores can be observed in both axial and parallel views within the sample CHA-1P and CHA-8P. From axial view, the pores are randomly distributed. Meanwhile, in parallel view, the pores channels (circled in red) formed within the particles, confirming the presence of ordered interconnected pore structures that is a typical pore characteristic resulting from self-assembly mechanism of non-ionic surfactants. Dark lines that circles in red observed in the parallel view of HRTEM images in

Figure **4** (a) and (b) represent the boundaries of pore channels formed within the spherical-like carbonated hydroxyapatite particles.

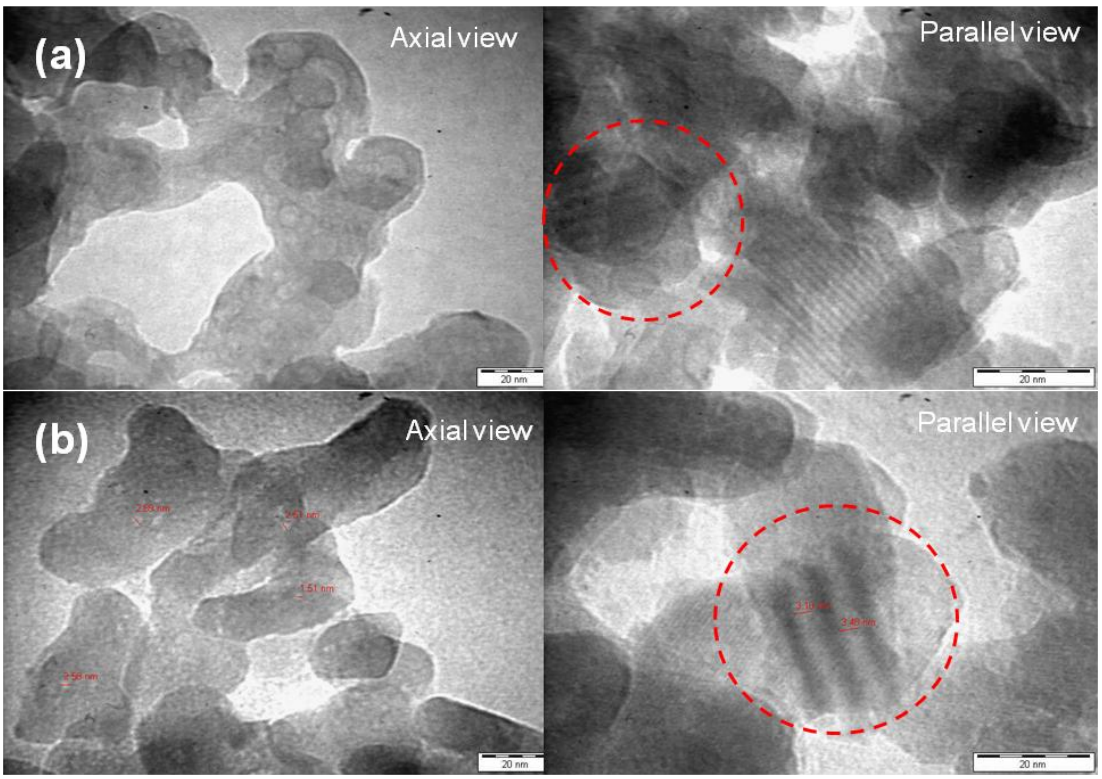

Figure 4. TEM micrographs of (a) CHA-1P and (b) CHA-8P from axial and parallel view.

Nitrogen adsorption desoprtion analysis was then conducted to investigate the effect of surfactant concentration on the pore size and surface area of nanoparticles. The nitrogen adsorption-desorption isotherms of the samples are shown in
Figure **5**. CHA-1P, CHA-4P, CHA-6P and CHA-8P exhibit the type IV isotherms with H1 hysteresis loop as shown in
Figure **5**. Porous materials that made of agglomerates or compacts of approximately uniform spheres in a fairly regular array usually characterised by this type of hysteresis loop [35]. The isotherm curve of CHA-0P is identified as type II isotherm, which is the common form isotherm of non-porous materials.

The inset graphs in
Figure **5** shows the corresponding BJH pore size distribution (PSD) curve. The pore sizes for CHA-1P are mainly distributed at 27.1 and 28.6 nm, while CHA-8P is mainly distributed at 20.8 and 25.3 nm. CHA-0P demonstrated a very low pore volume compared to other samples with the BJH pore size of 8.9 nm that most probably due to inter-particulate pores between the particles.

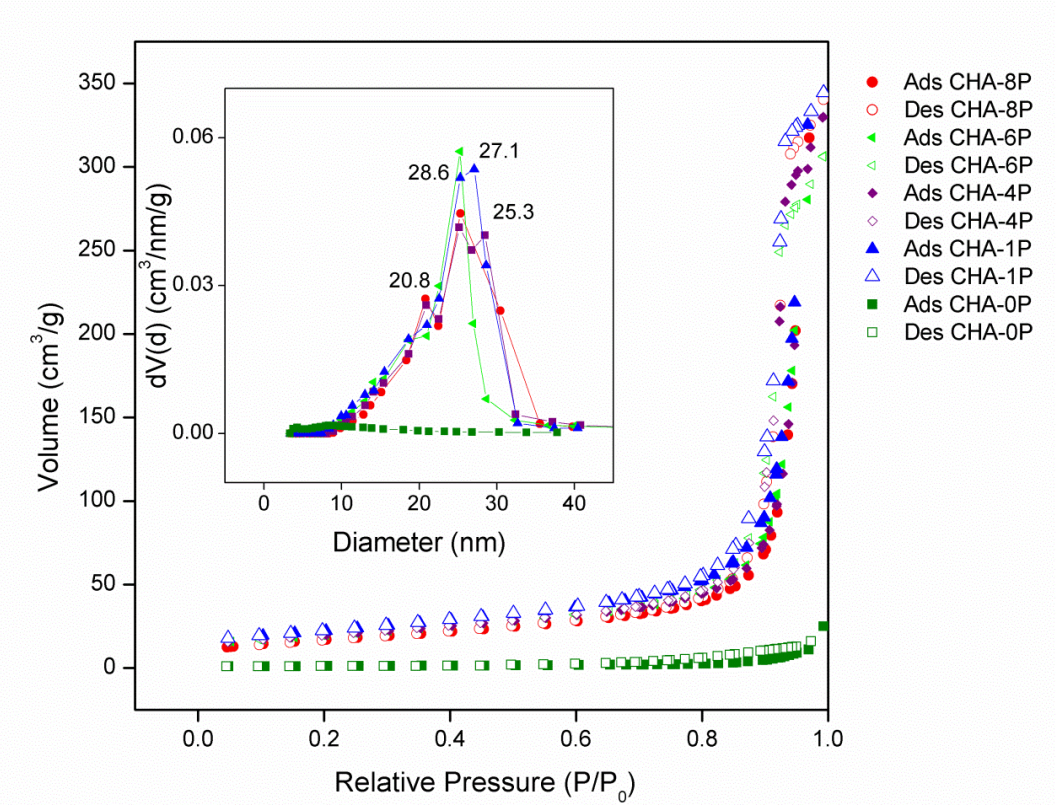

Figure 5. N_2 adsorption-desorption isotherms and BJH pore size distribution (inset graph) of CHA-0P, CHA-1P, CHA-4P, CHA-6P and CHA-8P.

Sample CHA-1P demonstrated the highest surface area (78 m^2g^{-1}), pore size (27 nm) and pore volume (0.542 cm^3/g) compared to other samples (Table 2). CHA-0P has the lowest surface area because porous structure could not be created without the surfactant presence. Meanwhile there is no significant difference in surface area of CHA-4P (63 m^2g^{-1}), CHA-6P (63 m^2g^{-1}) and CHA-8P (65 m^2g^{-1}). Sample CHA-1P exhibited the highest surface area since the concentration of surfactant solution during synthesis process (1.7 x 10^{-3} M) is the closest to the critical micelle concentration (CMC) (i.e. a concentration at which micelle start forming [36]) of P123. The CMC for P123 in the aqueous solution is 4.4 x 10^{-6} M [33]. Thus, if the surfactant concentration is maintain or close to CMC it is expected much more micelles are formed compared to those at higher or lower concentration. Instead of higher concentration of surfactant, the right system combination is more important to form micelles and porous structure. Increase number of micelles lead to increase in number of pores as well as surface area.

Table 2 Pore properties CHA-0P, CHA-1P CHA-4P, CHA-6P and CHA-8P

Sample	Concentration of P123 (mM)	Surface area, S_{BET} (m^2g^{-1})	Pore size, *BJH* (nm)	Pore volume (cm^3/g)
CHA-0P	0	4	8.9	0.041
CHA-1P	1.7	78	27.0	0.542
CHA-4P	7	63	25.2	0.523
CHA-6P	10	63	25.2	0.478
CHA-8P	14	65	26.1	0.541

TEM analysis was then conducted to verify the presence of mesopores within the nanoparticles. The pores are randomly distributed and not in precisely ordered alignment as view from the axial direction (

Figure **4**). However, through the parallel view, the pores channels (
Figure **4**: circled in red) observed to be formed within the nanoparticles that verify the existence of ordered pore structures due to self-assembly mechanism of non-ionic surfactants. The mesopores in sample CHA-1P are measured visually using TEM and estimated to be 3.8 nm in diameter while samples CHA-8P are slightly smaller, 3.1 nm in diameter. This value is within the region of mesopore size (2-50 nm) which confirm the formation of mesopore (brighter region) within the samples.
The apparent pore size observed in previous TEM images are not in agreement with the pore diameter determined using nitrogen adsorption (BJH). This is because the TEM analysis is focusing only on a smaller segregate region of the bulk sample while BJH analyse the whole bulk sample. Nevertheless, the pore sizes synthesise using lower and higher concentration of surfactant generally matches the IUPAC definition for mesopores (2-50 nm).

4. CONCLUSIONS

Mesoporous carbonated hydroxyapatite (CHA) was successfully synthesised by soft-templating hydrothermal method using non-ionic surfactant P123 as pore templates. The addition of P123 surfactant during synthesis of mesoporous CHA did not affect the phase purity of the mesoporous CHA however was thought to disturb the long-range order of the crystal structure and thus, resulting a lower crystallinity material. Concentration of surfactant affected the pore characteristics (i.e., surface area, pore size and pore volume) of mesoporous CHA. The highest surface (78 m^2g^{-1}) area was obtained when using 1.7 mM of P123. The optimum pore characteristics (i.e., surface area, pore size and pore volume) of mesoporous CHA obtained when surfactant concentration is maintain or close to critical micelle concentration (CMC). Thus, instead of higher concentration of surfactant, the right system combination is more important to form micelles and porous structure.

ACKNOWLEDGMENT

Authors would like to thanks Universiti Sains Malaysia that financially supported this research through Research University-Postgraduate Research Grant (RU-PRGS, 1001/PBAHAN/8046030).

REFERENCES

[1] Q. Zhao, T. Wang, J. Wang, L. Zheng, T. Jiang, G. Cheng, S. Wang, Fabrication of mesoporous hydroxycarbonate apatite for oral delivery of poorly water-soluble drug carvedilol, J. Non-Cryst. Solids **358**, 2 (2012) 229-235.
[2] N.F. Mohammad, R. Othman, F.Y. Yeoh, Controlling the pore characteristics of mesoporous apatite materials: Hydroxyapatite and carbonate apatite, Ceram. Int. **41**, 9, Part A (2015) 10624-10633.
[3] C. Rey, V. Renugopalakrishman, B. Collins, M.J. Glimcher, Fourier transform infrared spectroscopic study of the carbonate ions in bone mineral during aging, Calcif. Tissue Int. **49**, 4 (1991) 251-258.
[4] A. Krajewski, M. Mazzocchi, P.L. Buldini, A. Ravaglioli, A. Tinti, P. Taddei, C. Fagnano, Synthesis of carbonated hydroxyapatites: efficiency of the substitution and critical evaluation of analytical methods, Journal of Molecular Structure **744–747** (2005) 221-228.
[5] A. Bigi, G. Cojazzi, S. Panzavolta, A. Ripamonti, N. Roveri, M. Romanello, K. Noris Suarez, L. Moro, Chemical and structural characterization of the mineral phase from cortical and trabecular bone, J. Inorg. Biochem. **68**, 1 (1997) 45-51.
[6] N.F. Mohammad, R. Othman, F. Yee-Yeoh, Nanoporous hydroxyapatite preparation methods for drug delivery applications, Reviews on Advanced Materials Science **38**, 2 (2014) 138-147.

[7] Y. Guo, Y. Zhou, D. Jia, H. Tang, Fabrication and characterization of hydroxycarbonate apatite with mesoporous structure, Microporous Mesoporous Mater. **118**, 1-3 (2009) 480-488.
[8] Y.-P. Guo, T.-S. Lin, Y. Zhou, D.-C. Jia, Y.-J. Guo, Fabrication of monodisperse mesoporous hydroxycarbonate apatite microspheres by emulsion method, Microporous Mesoporous Mater. **127**, 3 (2010) 245-249.
[9] Y.-P. Guo, Y.-b. Yao, C.-Q. Ning, Y.-J. Guo, L.-F. Chu, Fabrication of mesoporous carbonated hydroxyapatite microspheres by hydrothermal method, Mater. Lett. **65**, 14 (2011) 2205-2208.
[10] Y.P. Guo, L.H. Guo, Y.B. Yao, C.Q. Ning, Y.J. Guo, Magnetic mesoporous carbonated hydroxyapatite microspheres with hierarchical nanostructure for drug delivery systems, Chem. Commun. (Camb.) **47**, 44 (2011) 12215-7.
[11] Y.-P. Guo, Y.-B. Yao, Y.-J. Guo, C.-Q. Ning, Hydrothermal fabrication of mesoporous carbonated hydroxyapatite microspheres for a drug delivery system, Microporous Mesoporous Mater. **155**, 0 (2012) 245-251.
[12] Y.-J. Guo, Y.-Y. Wang, T. Chen, Y.-T. Wei, L.-F. Chu, Y.-P. Guo, Hollow carbonated hydroxyapatite microspheres with mesoporous structure: Hydrothermal fabrication and drug delivery property, Mater. Sci. Eng., C **33**, 6 (2013) 3166-3172.
[13] Y.J. Guo, T. Long, W. Chen, C.Q. Ning, Z.A. Zhu, Y.P. Guo, Bactericidal property and biocompatibility of gentamicin-loaded mesoporous carbonated hydroxyapatite microspheres, Materials science & engineering. C, Materials for biological applications **33**, 7 (2013) 3583-91.
[14] T. Long, Y.-P. Guo, S. Tang, Y.-J. Guo, Z.-A. Zhu, Emulsion fabrication of magnetic mesoporous carbonated hydroxyapatite microspheres for treatment of bone infection, RSC Advances **4**, 23 (2014) 11816-11825.
[15] J. Rouquerol, D. Avnir, C.W. Fairbridge, D.H. Everett, J.H. Haynes, N. Pernicone, J.D.F. Ramsay, K.S.W. Sing, K.K. Unger, Recommendations for the Characterization of Porous Solid, Pure Appl. Chem. **66**, 8 (1994) 1739-1758.
[16] N.F. Mohammad, R. Othman, N.A. Abdullah, F.Y. Yeoh, In vitro Evaluation of Mesoporous Carbonated Hydroxyapatite in MC3T3-E1 Osteoblast Cells, Procedia Chemistry **19**, 0 (2016) 259-266.
[17] X.S. Zhao, G.Q. Lu, Nanoporous Materials - An Overview, Imperial College Press, London, 2004.
[18] P. Hatto, ISO concensus definitions relevant to nanomaterials and nanotechnologies, 4th Annual Nano Safety for Success Dialogue, ISO TC 229 and BSI NTI/1 Nanotechnologies standardization committees (2011).
[19] M. Sadat-Shojai, M.-T. Khorasani, E. Dinpanah-Khoshdargi, A. Jamshidi, Synthesis methods for nanosized hydroxyapatite with diverse structures, Acta Biomater. **9**, 8 (2013) 7591-7621.
[20] J. Yao, W. Tjandra, Y.Z. Chen, K.C. Tam, J. Ma, B. Soh, Hydroxyapatite nanostructure material derived using cationic surfactant as a template, J. Mater. Chem. **13**, 12 (2003) 3053-3057.
[21] P.M.S.L. Shanthi, M. Ashok, T. Balasubramanian, A. Riyasdeen, M.A. Akbarsha, Synthesis and characterization of nano-hydroxyapatite at ambient temperature using cationic surfactant, Mater. Lett. **63**, 24-25 (2009) 2123-2125.
[22] Y. Li, W. Tjandra, K.C. Tam, Synthesis and characterization of nanoporous hydroxyapatite using cationic surfactants as templates, Mater. Res. Bull. **43**, 8-9 (2008) 2318-2326.
[23] G.J.d.A.A. Soler-Illia, E.L. Crepaldi, D. Grosso, C. Sanchez, Block copolymer-templated mesoporous oxides, Current Opinion in Colloid & Interface Science **8**, 1 (2003) 109-126.
[24] Y.F. Zhao, J. Ma, Triblock co-polymer templating synthesis of mesostructured hydroxyapatite, Microporous Mesoporous Mater. **87**, 2 (2005) 110-117.
[25] D. Zhao, J. Feng, Q. Huo, N. Melosh, G.H. Fredrickson, B.F. Chmelka, G.D. Stucky, Triblock Copolymer Syntheses of Mesoporous Silica with Periodic 50 to 300 Angstrom Pores, Science **279**, 5350 (1998) 548-552.
[26] E. Landi, A. Tampieri, G. Celotti, S. Sprio, Densification behaviour and mechanisms of synthetic hydroxyapatites, Journal of the European Ceramic Society **20** (2000) 2377-2387.
[27] H. Wang, L. Zhai, Y. Li, T. Shi, Preparation of irregular mesoporous hydroxyapatite, Mater. Res. Bull. **43**, 6 (2008) 1607-1614.

[28] B. Li, X. Liao, L. Zheng, H. He, H. Wang, H. Fan, X. Zhang, Preparation and cellular response of porous A-type carbonated hydroxyapatite nanoceramics, Mater. Sci. Eng., C **32**, 4 (2012) 929-936.
[29] Y. Wang, S. Zhang, K. Wei, N. Zhao, J. Chen, X. Wang, Hydrothermal synthesis of hydroxyapatite nanopowders using cationic surfactant as a template, Mater. Lett. **60**, 12 (2006) 1484-1487.
[30] Y. Wang, J. Chen, K. Wei, S. Zhang, X. Wang, Surfactant-assisted synthesis of hydroxyapatite particles, Mater. Lett. **60**, 27 (2006) 3227-3231.
[31] H. Zhang, M. Liu, H. Fan, X. Zhang, An efficient method to synthesize carbonated nano hydroxyapatite assisted by poly(ethylene glycol), Mater. Lett. **75**, 0 (2012) 26-28.
[32] M. Khalid, M. Mujahid, S. Amin, R.S. Rawat, A. Nusair, G.R. Deen, Effect of surfactant and heat treatment on morphology, surface area and crystallinity in hydroxyapatite nanocrystals, Ceram. Int. **39**, 1 (2013) 39-50.
[33] E.S. Lee, Y.T. Oh, Y.S. Youn, M. Nam, B. Park, J. Yun, J.H. Kim, H.-T. Song, K.T. Oh, Binary mixing of micelles using Pluronics for a nano-sized drug delivery system, Colloids and Surfaces B: Biointerfaces **82**, 1 (2011) 190-195.
[34] A. Ślósarczyk, Z. Paszkiewicz, C. Paluszkiewicz, FTIR and XRD evaluation of carbonated hydroxyapatite powders synthesized by wet methods, Journal of Molecular Structure (2005) 657-661.
[35] K.S.W. Sing, D.H. Everett, R.A.W. Haul, L. Moscou, R.A. Pierotti, J. Rouquerol, T. Siemieniewska, Reporting Physisorption Data For Gas/Solid Systems with Special Reference to the Determination of Surface Area and Porosity, Pure Appl. Chem. **57**, 4 (1985) 603-619.
[36] V. Singh, P. Khullar, P.N. Dave, N. Kaur, Micelles, mixed micelles, and application of polyoxypropylene (PPO)-polyoxyethylene (PEO)-polyoxypropylene (PPO) triblock polymers, International Journal of Industrial Chemistry **4**, 12 (2013) 2-18.